Optimized voltage-support operation of VSC considering converter limitations

Fill this

***Abstract*—Grid faults are unfortunate events that compromise power systems. With the increasing integration of renewables and their associated power electronics converters, the injected currents are controllable, but at the same time, they have to be limited so as not to damage the converter. This poses the challenge to determine the combination of currents that improves the voltages at the point of common coupling. In this paper, such an issue is approached from an optimization perspective. A formulation for the analysis of faults in a generic system is presented. Numerical cases involving one and two converters have been studied with different types and depths of short-circuit faults. The optimized solutions have been compared with the operation points obtained following grid-codes. Overall, the results indicate that injecting only reactive power is not always the preferable choice. However, grid codes can be regarded as near-optimal decision rules, since their solution only differs slightly from the optimal one.**

***Index Terms*—VSC, Grid-Support, Optimization, Asymmetrical Fault, Current Saturation**

I. Introduction

THE rise in renewable energies has been implemented with the inclusion of Voltage Source Converters (VSC) as a means of coupling energetic resources to the grid while providing controllability [1]–[3]. Adopting such power electronics equipment has induced a progressive shrinkage on synchronous generators' influence in power systems. The high flexibility of VSC control enables advanced grid-support control, which could enhance the system performance during the fault and ensure a fast recovery after the fault clearance. However, compared to electrical machines, VSCs cannot withstand overloads [4]. Such current-saturation modifies VSCs' operation modes and must be considered in the power system computational analysis.

Not only do currents have to be constrained to not exceed the limitations, but they also have to collaborate on improving the voltages [5]. This becomes visible when looking at the requirements imposed by Transmission System Operators (TSO) in its grid codes [6], [7]. Such requirements are recent, as they have emerged together with the incorporation of renewables. As a consequence, renewable power plants have to control active and reactive power nowadays [8]. Besides, power converters have to transiently provide support in case of short-circuit faults. The latter aspect is often referred to as low voltage ride through (LVRT) [9], [10]. The traditional approach to raise the voltage is to inject reactive current proportionally to the voltage droop [8], [11]. During the analysis of faults, it is often the case that voltages are decomposed into positive, negative, and zero sequence values. By doing so, the study of the fault is expected to be simplified, and in addition to that, some intuition can be built from inspecting the positive and negative sequence voltages. A concerning unbalanced fault is such that substantially decreases the positive sequence voltage with respect to the nominal voltage while the negative sequence voltage increases. Both sequences have to be thoroughly controlled by power converters, as discussed in [11], [12].

Nevertheless, for the most part, grid codes only require reactive power injection for voltage support during short-circuit faults [13], [14]. This is because transmission networks are often considered to have an inductive characteristic. The influence of the grid impedance on the system's optimized operation points is covered in [12], where the authors express the current injection as a function of the voltage and the impedances. A recursive relation between the voltage and the current is found, which invalidates the possibility of working with a closed-form expression from where to compute the optimal currents solution. Expressions of the same nature are proposed in [15], where instead of attempting to solve the optimization problem, a control parameter is introduced. This takes various values, but no analysis is carried out to determine the optimal choice. The effect of varying this control parameter is studied in [16], although it is not computed with a systematic approach, but rather, manually. Reference [17] proposes a maximum allowed support (MAS) control scheme that could provide the maximum voltage support and simultaneously satisfying the current limitations. This study does not explicitly indicate how the current is distributed among the real and the imaginary positive and negative sequence components, and variations in input parameters are rather limited. Another voltage support scheme is presented in [18], where the injected currents depend neither on the active power nor the filter resistance. In addition, positive and negative sequence grid voltage values are imposed, which facilitates the obtention of the steady-state current values. A variation of the grid code requirements is depicted in [19]. The authors found it to provide better results than conventional grid codes by dynamically adjusting the positive and negative sequence voltage's reference. However, a purely inductive system was considered for its calculation. The majority of the grid support strategies described above are compared and summarized in [20]. It is worth mentioning that the systems under study considered in these references include a single VSC. Further conclusions are expected to be extracted from examining case studies with multiple converters.

This paper proposes a methodology to identify the optimized system equilibrium point during the fault considering converters' current limitations. The optimized operation points

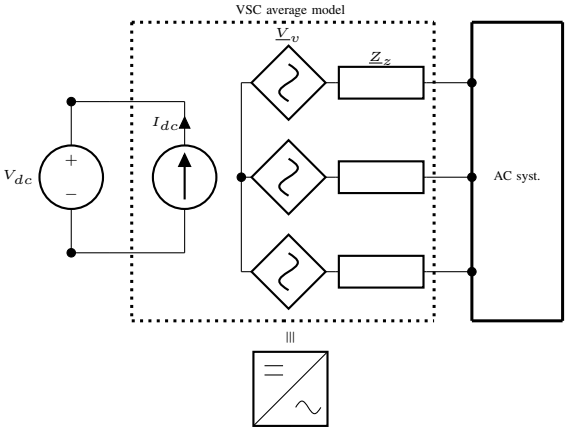

Fig. 1: Average model of a VSC connected to the grid

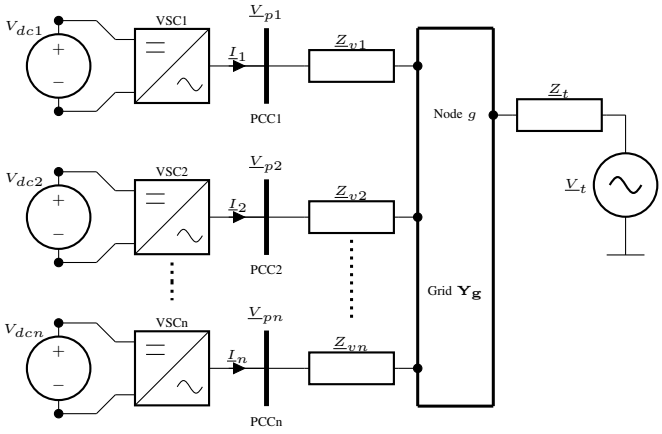

Fig. 2: Single-phase representation of a complete system

are compared with the results obtained from conventional grid codes. In these grid codes, two different strategies are implemented: one prioritizes positive sequence current whereas the other prioritizes negative sequence current. They are both restricted to only injecting reactive power. The optimized solution and the grid codes are tested for balanced and unbalanced faults, where this last category includes the line to ground and the line to line fault. First, a basic system with a single converter is studied. Then, the analysis is repeated for a system with two converters in order to identify their interaction.

This paper presents two main contributions. On the one hand, it indicates the preferable injected currents under diverse conditions. A deeper understanding of the optimality of the solutions is expected to be gained from it. On the other hand, comparisons between the optimal solution and the results obtained from grid codes are presented. According to the cases under study, the optimal results tend to differ more from grid codes in two-converter cases than in one-converter scenarios. An assessment about the convenience of grid codes to support faults can be derived, which should be useful when proposing future improvements in order to evolve towards more resilient grids.

II. Formulation

A. System modeling

VSCs are elements that interconnect DC systems with AC systems. As shown in Fig. 1, they can be modeled following the so-called average model. The VSC has been assumed to be connected to the AC grid with a filter in between denoted by $\underline{Z}_z$. The control strategy of the VSC consists of adjusting the voltages appropriately so that currents can indirectly meet the references [21].

Power systems are likely to involve more than a single converter. Therefore, the modeling is approached from a generalized perspective. Fig. 2 presents the generic modeling for a system with n converters. They are connected to a grid which has been split into a passive part, only formed by impedances and denoted by its admittance matrix $\mathbf{Y_g}$, and an active part, modeled with a Thevenin equivalent. A Norton equivalent would be valid as well, and in fact, it simplifies the formulation since it does not create an additional bus. Therefore, the mathematical model ends up using a Norton equivalent. The analysis of short-circuits faults can be performed in the natural reference frame or in symmetrical components as in [22]. For greater simplicity, in this paper, the circuits are modeled following the natural reference frame.

The VSCs are treated as current sources that inject currents of the form of $\mathbf{I_k}$ $\forall k \in [1, ..., n]$. These current vectors, expressed in the natural reference frame, are further developed as:

$$\mathbf{I_k} = \left[\underline{I}_k^a, \underline{I}_k^b, \underline{I}_k^c\right]^T \ . \tag{1}$$

Since this paper assumes VSCs to be connected to the system by only three wires, there is no zero sequence current. Thus, the formulation of the problem also imposes:

$$\underline{I}_k^a + \underline{I}_k^b + \underline{I}_k^c = 0 \ \forall k \in [1, ..., n] \ . \tag{2}$$

Additional impedances denoted by $\underline{Z}_{vk}$ connect the point of common coupling to the grid. Such point of common coupling is precisely where the voltages $\mathbf{V_{pk}}$ ought to be improved. Again, these vectors are constituted by the three phase voltages, that is:

$$\mathbf{V_{pk}} = \left[\underline{V}_{pk}^a, \underline{V}_{pk}^b, \underline{V}_{pk}^c\right]^T \ . \tag{3}$$

Voltages and currents are related via admittance submatrices of the form $\mathbf{Y_{vk}}$, which in normal operating conditions follow:

$$\mathbf{Y_{vk}} = \begin{pmatrix} \frac{1}{\underline{Z}_{vk}} & 0 & 0 \\ 0 & \frac{1}{\underline{Z}_{vk}} & 0 \\ 0 & 0 & \frac{1}{\underline{Z}_{vk}} \end{pmatrix} \ . \tag{4}$$

In case a fault occurs at the buses interconnected by $\underline{Z}_{vk}$, elements $1/\underline{Z}_f$ are added by observation, where $\underline{Z}_f$ denotes the fault impedance.

The admittance matrix $\mathbf{Y_g}$ is a $3n_g \times 3n_g$ matrix also built by observation, where n_g is the number of buses found in this passive $\mathbf{Y_g}$ grid. The vector $\mathbf{I_t}$ has dimensions $3 \times n_g$ and accounts for the injected currents into the grid $\mathbf{Y_g}$. All its elements are zero except for three entries that consider the currents from the Norton equivalent of the grid.

Consequently, the magnitudes depicted in Fig. 2 are finally related by:

$$\begin{pmatrix} \mathbf{I_1} \\ \mathbf{I_2} \\ \vdots \\ \mathbf{I_n} \\ \mathbf{I_t} \end{pmatrix} = \begin{pmatrix} \mathbf{Y_{v1}} & \mathbf{0} & \dots & \mathbf{0} & \mathbf{-Y'_{v1}} \\ \mathbf{0} & \mathbf{Y_{v2}} & \dots & \mathbf{0} & \mathbf{-Y'_{v2}} \\ \vdots & \vdots & \ddots & \vdots & \vdots \\ \mathbf{0} & \mathbf{0} & \dots & \mathbf{Y_{vn}} & \mathbf{-Y'_{vn}} \\ \mathbf{-Y'^{T}_{v1}} & \mathbf{-Y'^{T}_{v2}} & \dots & \mathbf{-Y'^{T}_{vn}} & \mathbf{Y_g} \end{pmatrix} \begin{pmatrix} \mathbf{V_{p1}} \\ \mathbf{V_{p2}} \\ \vdots \\ \mathbf{V_{pn}} \\ \mathbf{V_g} \end{pmatrix}, \tag{5}$$

where matrices of the form $\mathbf{Y'_{vk}}$ are $3 \times 3n_g$ objects constituted by zeros and only three $1/\underline{Z}_{vk}$ elements. For instance, considering $\underline{Z}_{v1}$ is connected to the first bus of the grid $\mathbf{Y}_g$, the corresponding $\mathbf{Y'_{v1}}$ matrix becomes:

$$\mathbf{Y'_{v1}} = \begin{pmatrix} \frac{1}{\underline{Z}_{v1}} & 0 & 0 & 0 & 0 & 0 & \dots & 0 & 0 & 0 \\ 0 & \frac{1}{\underline{Z}_{v1}} & 0 & 0 & 0 & 0 & \dots & 0 & 0 & 0 \\ 0 & 0 & \frac{1}{\underline{Z}_{v1}} & 0 & 0 & 0 & \dots & 0 & 0 & 0 \end{pmatrix}. \tag{6}$$

The final goal of the modeling is the obtention of voltages. They are computed from (5) by operating the product between the inverse of the full admittance matrix and the currents' vector. In order to have a clearer comprehension of the voltages, they are eventually converted into symmetrical components by means of Fortescue's transformation [23]:

$$\begin{pmatrix} \underline{V}^0_{pk} \\ \underline{V}^+_{pk} \\ \underline{V}^-_{pk} \end{pmatrix} = \frac{1}{3} \begin{pmatrix} 1 & 1 & 1 \\ 1 & \underline{a} & \underline{a}^2 \\ 1 & \underline{a}^2 & \underline{a} \end{pmatrix} \begin{pmatrix} \underline{V}^a_{pk} \\ \underline{V}^b_{pk} \\ \underline{V}^c_{pk} \end{pmatrix}, \tag{7}$$

where $\underline{a} = e^{j\frac{2\pi}{3}}$.

B. Optimization problem

Positive sequence voltages have to approach the nominal voltage while negative sequence voltages have to be minimized. The zero sequence component of the voltages is a magnitude likely to become non-null under asymmetrical faults. Nevertheless, as VSCs are unable to inject zero sequence currents, it will remain an uncontrolled variable in the sense that no efforts will be made towards reducing it. Current saturation restrictions imposed by the VSC characteristics have to be respected. This applies to each phase of each converter. Therefore, the generic optimization problem is expressed as:

$$\begin{aligned} \min \quad & \sum_{k=1}^{n} \left[\lambda_k^+ |(1 - V_{pk}^+)| + \lambda_k^- |(0 - V_{pk}^-)| \right], \\ \text{s.t.} \quad & \max\left(I_k^a, I_k^b, I_k^c\right) \leq I_{\text{max},k} \ \forall k \in [1, ..., n], \\ & \text{Eq. (5)}, \end{aligned} \tag{8}$$

where λ_k^+ and λ_k^- are weighting factors for positive and negative voltage magnitudes, the positive and negative sequence components of voltages $\underline{V}_{pk}$ are symbolically expressed as functions of the whole currents $\underline{I}$ involved in the system, and $I_{\text{max},k}$ is the maximum allowed current by the k converter for each phase. It has been assumed that voltages at each phase of the converter do not surpass the limitations, which seems a fair assumption considering that voltages decrease substantially during faults. This assumption is numerically validated in the case studies.

C. Grid code rules

In order to improve voltages during faults, grid code control rules typically impose injections of positive sequence currents proportional to the positive sequence voltage drop [8], [24]. When defined as generic piecewise functions:

$$\begin{cases} I_k^+ = 0 & V_{pk}^+ \geq V_{\text{high}}^+ \\ I_k^+ = k_p(V_{\text{high}}^+ - V_{pk}^+) & V_{\text{low}}^+ \leq V_{pk}^+ < V_{\text{high}}^+ \\ I_k^+ = I_{\text{max},k} & V_{pk}^+ < V_{\text{low}}^+ \end{cases} \tag{9}$$

The most basic of the four voltage support strategies analyzed in this paper, which will be denoted by GC, is precisely the application of (9). A similar proportionality can be established in the negative sequence:

$$\begin{cases} I_k^- = 0 & V_{pk}^- \leq V_{\text{low}}^- \\ I_k^- = k_n(V_{pk}^- - V_{\text{low}}^-) & V_{\text{low}}^- < V_{pk}^- \leq V_{\text{high}}^- \\ I_k^- = I_{\text{max},k} & V_{pk}^- > V_{\text{high}}^- \end{cases} \tag{10}$$

Constants k_p and k_n, which represent the slope of the droop, are set as fixed quantities. The unfavorable consequence of applying (9) and (10) simultaneously is that the nominal current of the converter could be exceeded. Indeed, during extreme faults, the positive sequence voltage could reach the lower threshold V_{low}^+ and the negative sequence voltage could surpass the upper threshold V_{high}^-. One way to fight against this problem can consist of injecting only positive or negative sequence currents; for example, the fundamental GC option only injects positive sequence current. However, this strategy is likely to be suboptimal. In case the voltages do not exceed these lower or upper thresholds, the converter would still be capable of injecting some current in the non-prioritized sequence up to reaching saturation.

One contribution of this paper is the proposal of a methodology to determine the available current margin.The two direct prioritizations are covered. One strategy is to have the positive sequence current following (9) and injecting the remaining maximum allowed current in the negative sequence. This methodology will be commonly referred to as GCP. The other option, abbreviated as GCN, is concerned with obeying (10) and analogously injecting the maximum positive sequence current that respects the limits. During all situations, the converters work under saturated conditions (current limits reached) as the non-prioritized current is set to the allowed maximum. Also, only reactive power is injected. The procedure to determine the non-prioritized current is depicted below.

Consider a generic distribution of positive and negative sequence voltages in the complex plane, as in Fig. 3. Phase currents are related to zero, positive, and negative sequence components by

$$\begin{pmatrix} \underline{I}^a \\ \underline{I}^b \\ \underline{I}^c \end{pmatrix} = \begin{pmatrix} 1 & 1 & 1 \\ 1 & \underline{a}^2 & \underline{a} \\ 1 & \underline{a} & \underline{a}^2 \end{pmatrix} \begin{pmatrix} \underline{I}^0 \\ \underline{I}^+ \\ \underline{I}^- \end{pmatrix} \tag{11}$$

where $\underline{I}^0$ is zero as the VSC is incapable of injecting it. The k index related to identifying a given VSC has been omitted

to alleviate the notation. Explicitly, (11) becomes:

$$\begin{cases} \underline{I}^a = \underline{I}^+ + \underline{I}^- \\ \underline{I}^b = \underline{a}^2\underline{I}^+ + \underline{a}\underline{I}^- \\ \underline{I}^c = \underline{a}\underline{I}^+ + \underline{a}^2\underline{I}^- \end{cases} \tag{12}$$

The goal is to determine the maximum current that respects the limitations. To do so, all three phase currents are set to the maximum allowed current. It is known beforehand that not all three phases will operate at saturation. Yet, one can imagine that if currents are gradually increased, one phase will reach saturation before the others. This will act as the most restrictive option. Consequently, the phase currents in (12) are squared in order to express them as functions of I_{re}^+, I_{im}^+, I_{re}^- and I_{im}^-:

$$\begin{cases} I_{\text{max}}^2 = (I_{re}^+ + I_{re}^-)^2 + (I_{im}^+ + I_{im}^-)^2 \\ I_{\text{max}}^2 = (-\frac{1}{2}I_{re}^+ + \frac{\sqrt{3}}{2}I_{im}^+ - \frac{1}{2}I_{re}^- - \frac{\sqrt{3}}{2}I_{im}^-)^2 \\ \qquad +(-\frac{1}{2}I_{im}^+ - \frac{\sqrt{3}}{2}I_{re}^+ - \frac{1}{2}I_{im}^- + \frac{\sqrt{3}}{2}I_{re}^-)^2 \\ I_{\text{max}}^2 = (-\frac{1}{2}I_{re}^+ - \frac{\sqrt{3}}{2}I_{im}^+ - \frac{1}{2}I_{re}^- + \frac{\sqrt{3}}{2}I_{im}^-)^2 \\ \qquad +(\frac{\sqrt{3}}{2}I_{re}^+ - \frac{1}{2}I_{im}^+ - \frac{\sqrt{3}}{2}I_{re}^- - \frac{1}{2}I_{im}^-)^2 \end{cases} \tag{13}$$

It is also convenient to define the angles of the positive and negative sequence currents, which are α^+ and α^- respectively:

$$\begin{cases} \alpha^+ = \angle(\underline{V}^+) - \frac{\pi}{2} \\ \alpha^- = \angle(\underline{V}^-) + \frac{\pi}{2} \end{cases} \tag{14}$$

where $\angle$ denotes the function that extracts the angle of a complex magnitude. By shifting the angles of the currents $\pm\frac{\pi}{2}$ rad with respect to the corresponding voltage, only reactive power is injected.

A procedure to find the four components I_{re}^+, I_{im}^+, I_{re}^- and I_{im}^- from (13) is described step-by-step. Algorithm 1 contains the methodology to be employed when the positive sequence is prioritized (GCP).

Algorithm 1 Current calculation for the GCP strategy

Input: $\underline{V}^+$, $\underline{V}^-$
Output: I_{re}^+, I_{im}^+, I_{re}^-, I_{im}^-

1: Compute α^+ and α^- from (14).
2: Use (9) to find I^+. Since α^+ is known, I_{re}^+ and I_{im}^+ are directly found.
3: Substitute I_{im}^- by $I_{re}^-\tan(\alpha^-)$ in (13) and solve the three equations for I_{re}^-.
4: Group the six solutions (two for each equation) as $[I_{re}^{a1-}, I_{re}^{a2-}, I_{re}^{b1-}, I_{re}^{b2-}, I_{re}^{c1-}, I_{re}^{c2-}]$.
5: Since $I_{im}^- = \tan(\alpha^-)I_{re}^-$, calculate the six associated currents $[I_{im}^{a1-}, I_{im}^{a2-}, I_{im}^{b1-}, I_{im}^{b2-}, I_{im}^{c1-}, I_{im}^{c2-}]$.
6: Select the three pairs of currents placed in the correct quadrant according to the value of α^-. Denote them by $[I_{re}^{a-}, I_{re}^{b-}, I_{re}^{c-}]$ and $[I_{im}^{a-}, I_{im}^{b-}, I_{im}^{c-}]$.
7: Compute currents $\underline{I}^{a-} = I_{re}^{a-} + jI_{im}^{a-}$, $\underline{I}^{b-} = I_{re}^{b-} + jI_{im}^{b-}$ and $\underline{I}^{c-} = I_{re}^{c-} + jI_{im}^{c-}$.
8: Finally, $I^- = \min\left(I^{a-}, I^{b-}, I^{c-}\right)$. Currents I_{re}^- and I_{im}^- are directly calculated as α^- has already been found.
9: **return** I_{re}^+, I_{im}^+, I_{re}^-, I_{im}^-.

Similarly, Algorithm 2 details the procedure to follow in case the negative sequence is prioritized (GCN).

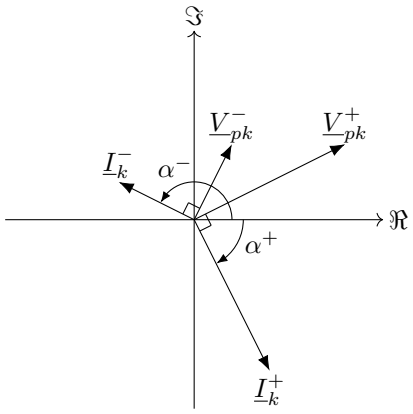

Fig. 3: Overview of positive and negative sequence voltages and currents following grid code rules

Algorithm 2 Current calculation for the GCN strategy

Input: $\underline{V}^+$, $\underline{V}^-$
Output: I_{re}^+, I_{im}^+, I_{re}^-, I_{im}^-

1: Compute α^+ and α^- from (14).
2: Use (10) to find I^-. Since α^- is known, I_{re}^- and I_{im}^- are directly found.
3: Substitute I_{im}^+ by $I_{re}^+\tan(\alpha^+)$ in (13) and solve the three equations for I_{re}^+.
4: Group the six solutions (two for each equation) as $[I_{re}^{a1+}, I_{re}^{a2+}, I_{re}^{b1+}, I_{re}^{b2+}, I_{re}^{c1+}, I_{re}^{c2+}]$.
5: Since $I_{im}^+ = \tan(\alpha^+)I_{re}^+$, calculate the six associated currents $[I_{im}^{a1+}, I_{im}^{a2+}, I_{im}^{b1+}, I_{im}^{b2+}, I_{im}^{c1+}, I_{im}^{c2+}]$.
6: Select the three pairs of currents placed in the correct quadrant according to the value of α^+. Denote them by $[I_{re}^{a+}, I_{re}^{b+}, I_{re}^{c+}]$ and $[I_{im}^{a+}, I_{im}^{b+}, I_{im}^{c+}]$.
7: Compute currents $\underline{I}^{a+} = I_{re}^{a+} + jI_{im}^{a+}$, $\underline{I}^{b+} = I_{re}^{b+} + jI_{im}^{b+}$ and $\underline{I}^{c+} = I_{re}^{c+} + jI_{im}^{c+}$.
8: Finally, $I^+ = \min\left(I^{a+}, I^{b+}, I^{c+}\right)$. Currents I_{re}^+ and I_{im}^+ are directly calculated as α^+ has already been found.
9: **return** I_{re}^+, I_{im}^+, I_{re}^-, I_{im}^-.

III. Single converter case study

The analysis is first performed considering a one-converter case study as the one depicted in Fig. 4. A fault is forced at the point of connection of the grid. The impedances that model the fault are set accordingly to the type of fault, i.e., balanced or unbalanced (line to ground or line to line). Double line to ground faults are not covered in this study, not because they are unfeasible to be analyzed, but because there is a direct connection between the two faulted phases. This causes variations from a parametric study to have an almost null influence on the results. In any case, the goal is to improve the voltage $\underline{V}_{p1}$ by injecting the optimal $\underline{I}_1^a$, $\underline{I}_1^b$ and $\underline{I}_1^c$ currents.

Three parametric studies are performed. One considers variations in the fault impedance. This case is explicitly described in order to exemplify the formulation. Another study analyzes a varying R_1/X_1 ratio, which stands for the proportion between the resistive and the inductive parts that compose the

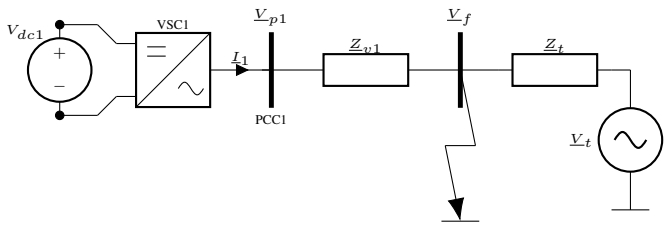

Fig. 4: Single-phase representation of the single converter system under study

impedance $\underline{Z}_{v1}$. This ratio is modified while the absolute value of the impedance is kept constant. The third case presents the effect of increasing the distance of a hypothetical submarine cable. Regarding the grid codes, the values of the constants are gathered in Table IV. They remain the same for all studies. The results gathered in this paper are computed with Python 3.9.1 using the Mystic package, a highly constrained non-convex optimization framework [25], [26]. A differential global optimization solver has been employed with a relative precision up to $1 \cdot 10^{-6}$.

A. Fault impedance variation analysis

For a single converter system as the one depicted in Fig. 4, the fault impedance connected to the bus at voltage $\underline{V}_f$ represents the event of short-circuit in this case. Explicitly, voltages and currents are related by:

$$\begin{pmatrix} \underline{I}_1^a \\ \underline{I}_1^b \\ \underline{I}_1^c \\ \underline{I}_t^a \\ \underline{I}_t^b \\ \underline{I}_t^c \end{pmatrix} = (\mathbf{Y_v} + \mathbf{Y_f}) \begin{pmatrix} \underline{V}_{p1}^a \\ \underline{V}_{p1}^b \\ \underline{V}_{p1}^c \\ \underline{V}_f^a \\ \underline{V}_f^b \\ \underline{V}_f^c \end{pmatrix}, \tag{15}$$

where the admittance matrix has been split into two parts: $\mathbf{Y_v}$ represents the non-faulted admittance matrix of the system, whereas $\mathbf{Y_f}$ is constituted by the admittances that intervene in the fault and has the same size as $\mathbf{Y_v}$. The short-circuit impedance is included as the corresponding elements in $\mathbf{Y_f}$ while other elements are equal to 0. This way, the admittance matrices are defined as:

$$\mathbf{Y_v} = \left(\begin{array}{ccc|ccc} \underline{Y}_{v1} & 0 & 0 & -\underline{Y}_{v1} & 0 & 0 \\ 0 & \underline{Y}_{v1} & 0 & 0 & -\underline{Y}_{v1} & 0 \\ 0 & 0 & \underline{Y}_{v1} & 0 & 0 & -\underline{Y}_{v1} \\ \hline -\underline{Y}_{v1} & 0 & 0 & \underline{Y}_{v1} + \underline{Y}_t & 0 & 0 \\ 0 & -\underline{Y}_{v1} & 0 & 0 & \underline{Y}_{v1} + \underline{Y}_t & 0 \\ 0 & 0 & -\underline{Y}_{v1} & 0 & 0 & \underline{Y}_{v1} + \underline{Y}_t \end{array}\right) \tag{16}$$

where $\underline{Y}_{v1} = 1/\underline{Z}_{v1}$ and $\underline{Y}_t = 1/\underline{Z}_t$.

On the other hand, the fault admittance $\mathbf{Y_f}$ is fully dependent on the fault, and therefore, it is built by observation. The optimization problem for the one case converter reads:

$$\begin{aligned} \min \quad & \lambda_1^+ |(1 - V_{p1}^+)| + \lambda_1^- |(0 - V_{p1}^-)| \ , \\ \text{s.t.} \quad & \max(I_1^a, I_1^b, I_1^c) \leq I_{\text{max,1}} \ , \\ & \text{Eq. (15)} \ , \end{aligned} \tag{17}$$

Because of the nature of the converter, it is also imposed that the sum of the three-phase currents becomes null. The procedure to solve the optimization problem is first responsible for initializing the admittances matrices $\mathbf{Y_v}$ as in (16), and then, constructing $\mathbf{Y_f}$. Next, currents are initialized to a random array of values, for instance. The Mystic package is subsequently called to solve the optimization problem stated in (17) up to a given relative precision $\delta = 1 \cdot 10^{-6}$. Positive and negative sequence voltages are evaluated to determine the optimality of the solution by means of (7). In the case of sweeping a range of n scenarios with different fault impedance values, this process is repeated n times. Currents are eventually also transformed to positive and negative sequence values since the final goal is to evaluate their values in this frame of reference. Unless noted otherwise, the corresponding baseline parameters of the system in Fig. 4 are indicated in Table I.

TABLE I: System parameters for the one-converter case

Parameter	Value
$\underline{V}_t$	1.00
I_{max}	1.00
$\underline{Z}_{v1}$	$0.01 + j0.05$
$\underline{Z}_t$	$0.01 + j0.1$
$[\lambda_1^+, \lambda_1^-]$	$[1, 1]$

Solving the problem with the aforementioned steps for a balanced fault yields the results shown in Fig. 5, where impedance $\underline{Z}_x$ denotes the fault impedance connected to each phase. It has been considered to be fully resistive. The results suggest that the OPT case is the preferred one, as its associated objective function is always the smallest, as expected. This optimal solution is achieved by distributing the currents between the real and imaginary parts. The imaginary current remains slightly larger than the real current (in absolute value). This is the main difference between OPT and the grid code implementation found in GCP and GCN. These two strategies always specify a null real current in both sequences, and in this case, the converter employs the full capability for the imaginary positive sequence current. Therefore, their objective functions and voltage profiles become identical in this case with a balanced fault.

Significantly different results are obtained in the case of a line to line fault, as shown in Fig. 6. This unbalanced fault causes the optimal currents to be almost null in the positive sequence, so the majority of the current capability is employed for the negative sequence. Severe faults require a large real current (in absolute value), whereas in the case of less extreme faults, the imaginary current tends to the maximum, i.e, 1. Even though the real current is kept at zero for GCP and GCN, their imaginary currents vary significantly across the range of Z_x values. GCP tends to approach the results provided by OPT for large Z_x, whereas GCN evolves on the contrary direction. That is, for low fault impedances, GCP prioritizes injecting current in the positive sequence whereas GCN does the same for the negative sequence, as expected. As a consequence, positive sequence voltages in the case of GCP are initially superior to the ones obtained with GCN, and the contrary applies to the negative sequence voltages. The situation is reversed around $Z_x \approx 0.1$. Since the fault is not that severe, much of the current capability is employed in the non-prioritized sequence in order to reach saturation. In the end, there is an almost constant minimal

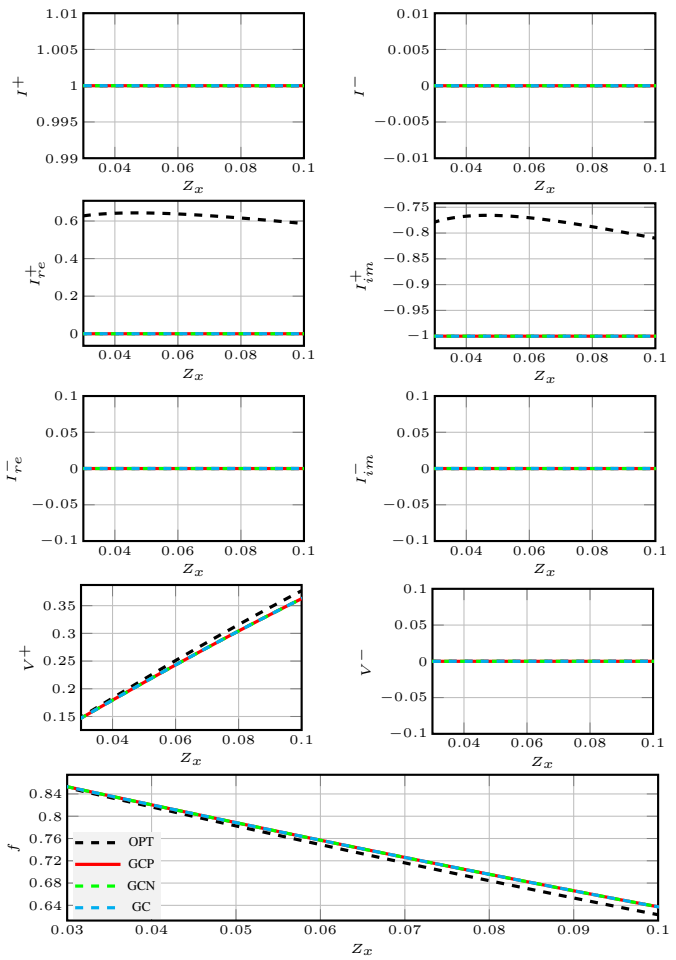

Fig. 5: Influence of the currents for a balanced fault with a varying fault impedance, one-converter case

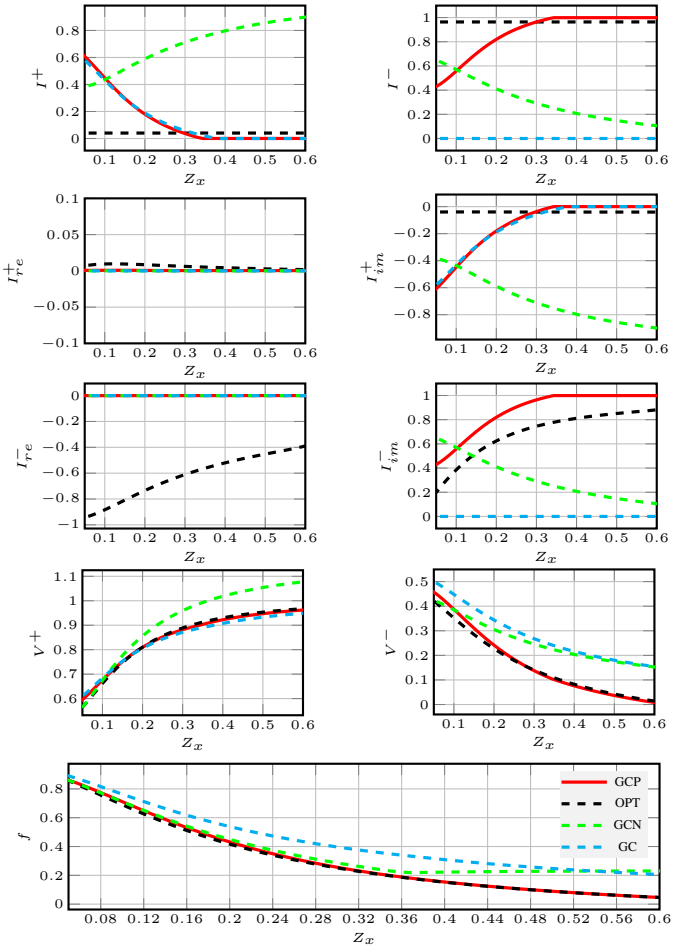

Fig. 6: Influence of the currents for a line to line fault with a varying fault impedance, one-converter case

difference between OPT and GCP, as their objective functions are nearly the same.

B. R_1/X_1 variation analysis

The R_1/X_1 variation analysis performs a swept for a range of a varying angle of the $\underline{Z}_{v1}$ impedance, while the absolute value is preserved. The goal of this study is to determine how this affects the distribution of currents between the real and the imaginary part. The results in Fig. 7 for the OPT case show that despite an increase in the resistive part of the impedance, the currents remain nearly constant for all the range of values. Most of the current capability is dedicated to I^+_{im} and I^-_{re}. The converter injects a non-negligible active power, as the injected complex power remains around $0.30 + j0.45$.

Differences among the objective functions of OPT, GCP and GCN are more significant for a large R_1/X_1 value due to the incapability of injecting real current from the converter. In particular, the OPT option achieves a larger positive sequence voltage than both GCP and GCN for all ranges of values. Although the negative sequence voltage obtained with OPT is initially larger, it is further reduced with increases in R_1/X_1, whereas this same voltage tends to grow for GCP and GCN. Despite the fact that GCP prioritizes active current, as the fault is not extreme and it has been imposed that the converter has to operate under saturated conditions, the GCP strategy injects more current in the negative sequence than in the positive sequence. The contrary applies to the GCN option. Therefore, GCN yields larger V^+ and V^- voltages compared to GCP. In the end, the objective function is practically the same for both options.

TABLE II: System parameters for the one-converter case

Parameter	Value	Units
$\underline{Z}_s$	$6.674 \cdot 10^{-5} + j2.597 \cdot 10^{-4}$	pu/km
$\underline{Z}_p$	$-j77.372$	pu·km

C. Cable length variation analysis

Fig. 8 represents the third parametric study regarding single converter systems, which deals with a hypothetical submarine cable modeled with its π equivalent. The data selected to model the cable are extracted from [27] and adapted to per-unit values, which are shown in Table II. The followed approach to analyze the system is identical to the previous ones, except for the reduction of the set of elements including the cable and the grid. The corresponding Thevenin equivalent is defined by:

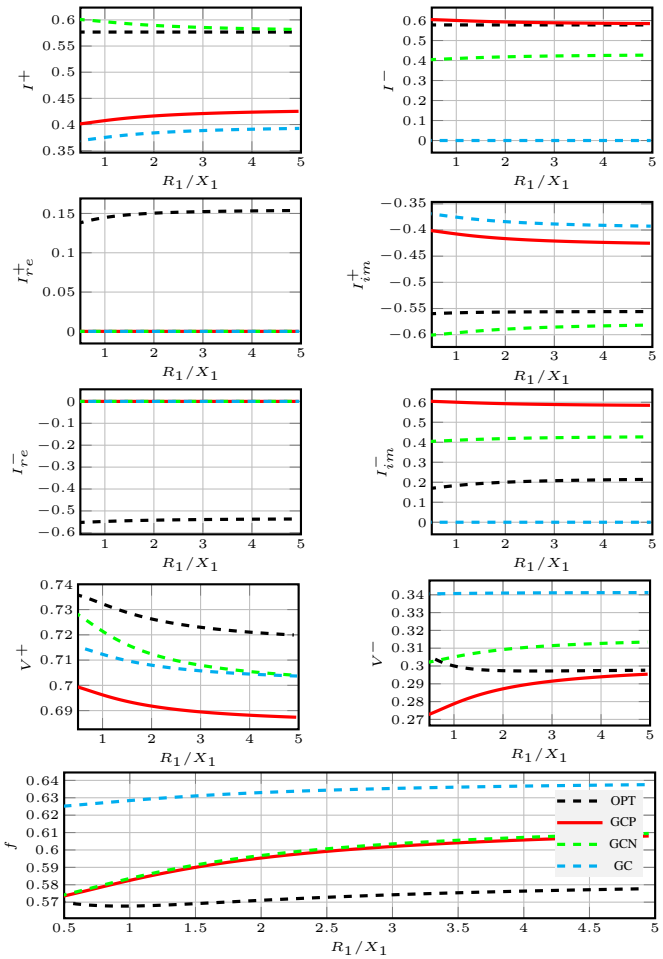

Fig. 7: Influence of the currents for the line to ground fault with a varying R_1/X_1 ratio and a fault impedance $\underline{Z}_{ag} = 0.01$, one-converter case

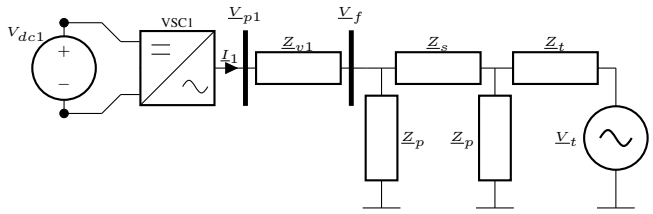

Fig. 8: Single-phase representation of the single converter connected to a system with a cable

$$\begin{cases} \underline{V}'_t = \dfrac{\underline{Z}_p\underline{Z}_p}{2\underline{Z}_t\underline{Z}_p+\underline{Z}_p\underline{Z}_s+\underline{Z}_p\underline{Z}_p+\underline{Z}_t\underline{Z}_s} \\ \underline{Z}'_t = \dfrac{\underline{Z}_p\underline{Z}_p\underline{Z}_t+\underline{Z}_p\underline{Z}_p\underline{Z}_s+\underline{Z}_p\underline{Z}_s\underline{Z}_t}{2\underline{Z}_p\underline{Z}_t+\underline{Z}_s\underline{Z}_p+\underline{Z}_s\underline{Z}_t+\underline{Z}_p\underline{Z}_p} \end{cases} \tag{18}$$

Similarly as before, a Norton equivalent is preferred. The current $\underline{I}'_t$ is simply equal to $\underline{V}'_t/\underline{Z}'_t$, which yields a basic system as the one in Fig. 4.

The analysis performed considers a cable with a varying length, up to 100 km. Its impact on the Thevenin equivalent parameters is shown in Fig. 9. The voltage experiences a subtle increase, while the imaginary part of the equivalent impedance

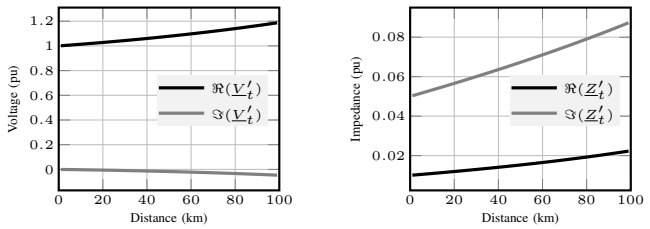

Fig. 9: Thevenin voltage and impedance depending on the cable distance

TABLE III: System parameters for the two converter case

Parameter	Value
$\underline{V}_t$	1.00
$I_{\max}$	1.00
$\underline{Z}_{v1}$	$0.01 + j0.05$
$\underline{Z}_{v2}$	$0.02 + j0.06$
$\underline{Z}_t$	$0.01 + j0.1$
$[\lambda_1^+, \lambda_1^-, \lambda_2^+, \lambda_2^-]$	$[1, 1, 1, 1]$

grows considerably with distance, yet the $\Re(\underline{Z}'_t)/\Im(\underline{Z}'_t)$ ratio tends to rise.

The options OPT, GCP and GCN are again evaluated, as depicted in Fig. 10. Increasing the cable distance causes the negative sequence voltage to grow, while the positive sequence voltage also tends to grow. This phenomenon mostly differs from the profiles obtained in Fig. 6 and 7, where both voltages either simultaneously approached the objective value (1 and 0 respectively), or distanced from it. Thus, it makes sense that larger distances imply a lower I^+_{im} current in the case of the grid code implementation, while the less convenient growing negative sequence voltages force an increment in I^-_{im}. Most of the current capability is precisely devoted to this negative sequence imaginary current. The OPT option achieves a more favorable objective function value than GCP and GCN by keeping the positive sequence currents practically constant, increasing I^-_{re} (in absolute value), and decreasing I^-_{im}, which is the inverse trend followed by GCP and GCN. Surprisingly, in the OPT case, the VSC would have to inject a tiny negative active power, that is, this active power flows from the grid to the converter.

IV. Two-converter case study

A case study with two VSCs is analyzed in this Section in order to spot the interaction between both converters and compare the performance of the optimization with the grid code rules. Fig. 11 shows a single-phase representation of the system under study. The converters are coupled to the grid by means of slightly different impedances $\underline{Z}_{v1}$ and $\underline{Z}_{v2}$, which causes different distributions of current. Table III shows their values together with other input data.

Analogous to the one-converter situation, the optimization

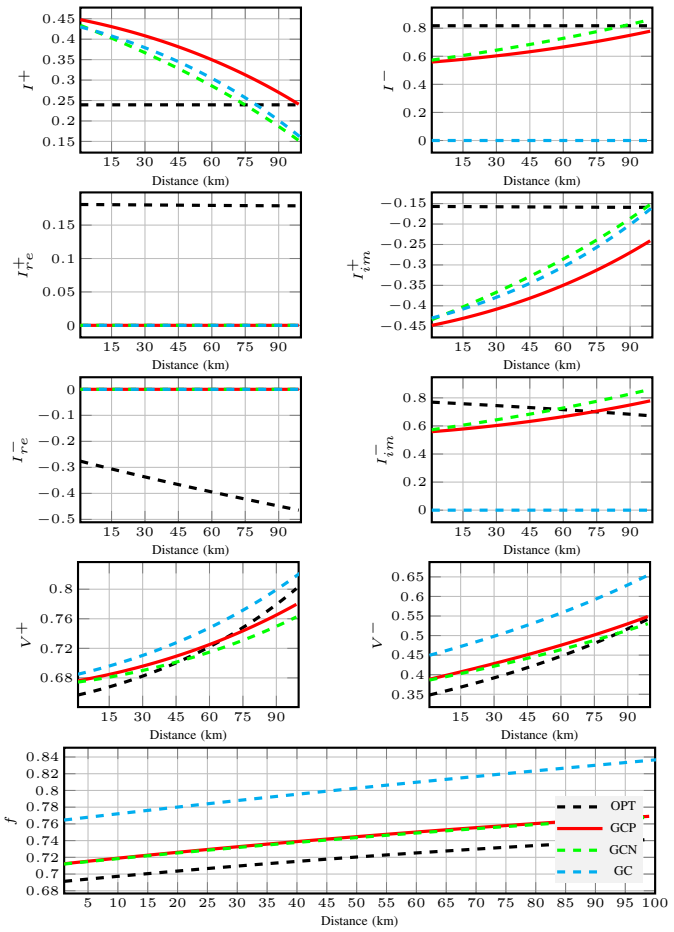

Fig. 10: Influence of the currents for a line to line fault with $\underline{Z}_{ab} = 0.1$ and a varying cable distance, one-converter case

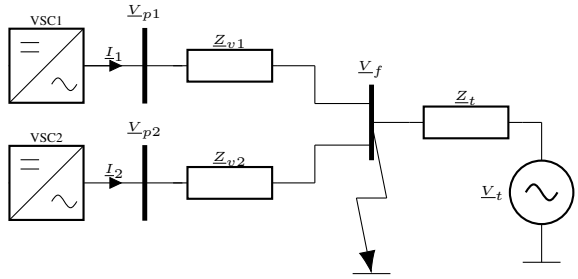

Fig. 11: Single-phase representation of the two-converter system under study

problem becomes:

$$\begin{aligned} \min \quad & \lambda_1^+|(1-V_{p1}^+)| + \lambda_1^-|(0-V_{p1}^-)| \\ & + \lambda_2^+|(1-V_{p2}^+)| + \lambda_2^-|(0-V_{p2}^-)|, \\ \text{s.t.} \quad & \max(I_1^a, I_1^b, I_1^c) \leq I_{\text{max},1} \ , \\ & \max(I_2^a, I_2^b, I_2^c) \leq I_{\text{max},2} \ , \\ & \text{Particular Eq. (5)} \ , \end{aligned} \tag{19}$$

where the dependence of the currents on the voltages has been omitted. The application of the grid-code is the same as before, in the sense that the injection of current $\underline{I}_1$ only depends on

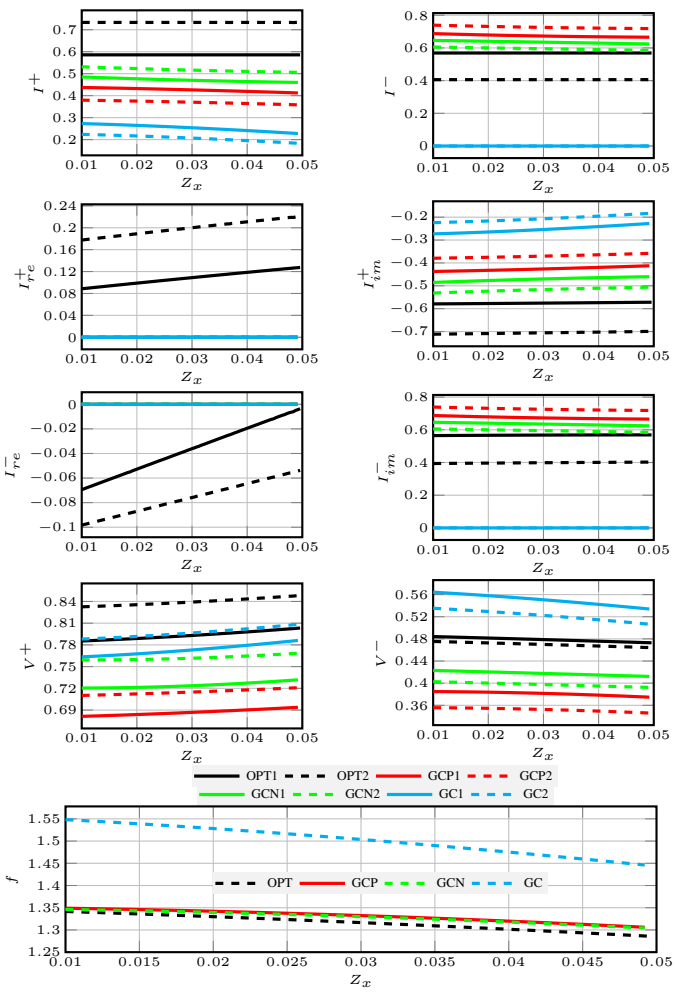

Fig. 12: Influence of the currents for the line to line fault with a varying fault impedance in bus 8 of the IEEE 9-bus system

$\underline{V}_{p1}$, and $\underline{I}_2$ is expressed as a function of $\underline{V}_{p2}$ respectively following the grid-code.

A. Fault impedance variation analysis

V. Conclusion

This paper has proposed an optimization scheme to improve the grid voltage support during short-circuit faults. Such strategy has been compared with conventional grid codes, where either positive or negative currents are prioritized and the converter is forced to operate under saturation conditions by only injecting reactive power. Several parameters have been swept, such as the fault impedance, the angle of the interconnecting impedance, and the length of a submarine cable, either for one or two-converter cases. In most situations, the distribution of currents derived from the optimization differs considerably from the currents injected following the grid codes. Yet, the optimization function, which in turn depends on the positive and negative sequence voltages, rarely improves by more than 10%. Differences are especially tiny for severe faults. Thus, this work concludes that there are no large improvements to be gained by employing other rules. Grid codes are already

near-optimal choices, even if the converter is only injecting reactive power/current.

ACKNOWLEDGMENT

Fill this.

APPENDIX

TABLE IV: Grid code parameters

Parameter	Value
V^+_{high}	0.9
V^+_{low}	0.4
V^-_{high}	0.6
V^-_{low}	0.1
k_p	2.0
k_n	2.0

REFERENCES

[1] M. Imhof and G. Andersson, "Power system stability control using voltage source converter based hvdc in power systems with a high penetration of renewables," in *2014 Power Systems Computation Conference*. IEEE, 2014, pp. 1–7.

[2] S. Eren, A. Bakhshai, and P. Jain, "Control of three-phase voltage source inverter for renewable energy applications," in *2011 IEEE 33rd International Telecommunications Energy Conference (INTELEC)*. IEEE, 2011, pp. 1–4.

[3] F. Blaabjerg, Y. Yang, K. Ma, and X. Wang, "Power electronics-the key technology for renewable energy system integration," in *2015 International Conference on Renewable Energy Research and Applications (ICRERA)*. IEEE, 2015, pp. 1618–1626.

[4] A. Abdou, A. Abu-Siada, and H. Pota, "Improving the low voltage ride through of doubly fed induction generator during intermittent voltage source converter faults," *Journal of Renewable and Sustainable Energy*, vol. 5, no. 4, p. 043110, 2013.

[5] J. Morren, *Grid support by power electronic converters of Distributed Generation units*, 2006.

[6] I. Erlich, W. Winter, and A. Dittrich, "Advanced grid requirements for the integration of wind turbines into the german transmission system," in *2006 IEEE Power Engineering Society General Meeting*. IEEE, 2006, pp. 7–pp.

[7] X. Zhang, Z. Wu, M. Hu, X. Li, and G. Lv, "Coordinated control strategies of vsc-hvdc-based wind power systems for low voltage ride through," *energies*, vol. 8, no. 7, pp. 7224–7242, 2015.

[8] M. Mohseni and S. M. Islam, "Review of international grid codes for wind power integration: Diversity, technology and a case for global standard," *Renewable and Sustainable Energy Reviews*, vol. 16, no. 6, pp. 3876–3890, 2012.

[9] M. Tsili and S. Papathanassiou, "A review of grid code technical requirements for wind farms," *IET Renewable power generation*, vol. 3, no. 3, pp. 308–332, 2009.

[10] J. Conroy and R. Watson, "Low-voltage ride-through of a full converter wind turbine with permanent magnet generator," *IET Renewable power generation*, vol. 1, no. 3, pp. 182–189, 2007.

[11] A. Haddadi, I. Kocar, J. Mahseredjian, U. Karaagac, and E. Farantatos, "Negative sequence quantities-based protection under inverter-based resources challenges and impact of the german grid code," *Electric Power Systems Research*, vol. 188, p. 106573, 2020.

[12] A. Camacho, M. Castilla, J. Miret, L. G. de Vicuña, and R. Guzman, "Positive and negative sequence control strategies to maximize the voltage support in resistive–inductive grids during grid faults," *IEEE Transactions on Power Electronics*, vol. 33, no. 6, pp. 5362–5373, 2017.

[13] Red Eléctrica de España. (2016) Información sobre implementación de códigos de red de conexión. textos de los códigos de red de conexió europeos. reglamento 2016/631. [Online]. Available: https://www.esios.ree.es/es/pagina/codigos-red-conexion

[14] A. G. Paspatis and G. C. Konstantopoulos, "Voltage support under grid faults with inherent current limitation for three-phase droop-controlled inverters," *Energies*, vol. 12, no. 6, p. 997, 2019.

[15] A. Camacho, M. Castilla, J. Miret, J. C. Vasquez, and E. Alarcon-Gallo, "Flexible voltage support control for three-phase distributed generation inverters under grid fault," *IEEE transactions on industrial electronics*, vol. 60, no. 4, pp. 1429–1441, 2012.

[16] X. Guo, X. Zhang, B. Wang, W. Wu, and J. M. Guerrero, "Asymmetrical grid fault ride-through strategy of three-phase grid-connected inverter considering network impedance impact in low-voltage grid," *IEEE Transactions on Power Electronics*, vol. 29, no. 3, pp. 1064–1068, 2013.

[17] M. M. Shabestary and Y. A.-R. I. Mohamed, "An analytical method to obtain maximum allowable grid support by using grid-connected converters," *IEEE Transactions on Sustainable Energy*, vol. 7, no. 4, pp. 1558–1571, 2016.

[18] Z. Dai, H. Lin, H. Yin, and Y. Qiu, "A novel method for voltage support control under unbalanced grid faults and grid harmonic voltage disturbances," *IET power Electronics*, vol. 8, no. 8, pp. 1377–1385, 2015.

[19] M. M. Shabestary and Y. A.-R. I. Mohamed, "Asymmetrical ride-through and grid support in converter-interfaced dg units under unbalanced conditions," *IEEE Transactions on Industrial Electronics*, vol. 66, no. 2, pp. 1130–1141, 2018.

[20] M. M. Shabestary, S. Mortazavian, and Y. I. Mohamed, "Overview of voltage support strategies in grid-connected vscs under unbalanced grid faults considering lvrt and hvrt requirements," in *2018 IEEE International Conference on Smart Energy Grid Engineering (SEGE)*. IEEE, 2018, pp. 145–149.

[21] M. T. Andani, H. Pourgharibshahi, Z. Ramezani, and H. Zargarzadeh, "Controller design for voltage-source converter using lqg/ltr," in *2018 IEEE texas power and energy conference (TPEC)*. IEEE, 2018, pp. 1–6.

[22] M. G. Taul, S. Golestan, X. Wang, P. Davari, and F. Blaabjerg, "Modeling of converter synchronization stability under grid faults: The general case," *IEEE Journal of Emerging and Selected Topics in Power Electronics*, 2020.

[23] C. L. Fortescue, "Method of symmetrical co-ordinates applied to the solution of polyphase networks," *Transactions of the American Institute of Electrical Engineers*, vol. 37, no. 2, pp. 1027–1140, 1918.

[24] National Grid, "The grid code, issue 6, revision 1," https://www.nationalgrideso.com/document/162271/download, 2021.

[25] M. M. McKerns, L. Strand, T. Sullivan, A. Fang, and M. A. Aivazis, "Building a framework for predictive science," *arXiv preprint arXiv:1202.1056*, 2012.

[26] M. McKerns, P. Hung, and M. Aivazis, "mystic: highly-constrained non-convex optimization and uq, 2009."

[27] M. Cheah, "Offshore wind integration through high voltage direct current systems," Ph.D. dissertation, Cardiff University, 2017.